# AERODYNAMIC VALIDATION OF rFlow3D CODE WITH UH-60A DATA INCLUDING HIGH ADVANCE RATIOS

Yasutada Tanabe, Japan Aerospace Exploration Agency, Tokyo, Japan
Hideaki Sugawara, Ryoyu Systems Co. Ltd., Nagoya, Japan

**Abstract**

Validation of the rFlow3D code developed at Japan Aerospace Exploration Agency (JAXA) has been carried out with the published UH-60A test data in hover and forward flight. Also, the slowed rotor conditions are simulated to investigate the applicability of this code at high advance ratios. Although the elastic deformation of the blade is not considered at this point, good agreement of the aerodynamic performance is obtained compared with the experimental data. Extensions of the CFD solver toward complete compound helicopter simulations are also discussed.

## 1. INTRODUCITON

High speed rotorcraft that can fly at a speed nearly twice of conventional helicopters has a very promising new market especially for EMS operations. A variety of configurations has been proposed and under development including the tilt rotor, and several types of compound helicopters. When missions including a significant part of hovering operations or low-speed flight, the compound helicopter design is considered more efficient than the tilt rotor. [1] Two types of compound helicopters are mainly under development. Co-axial rotors with a propeller such as Sikorsky's X2 [2-4] and single rotor with a wing and propellers such as Airbus Helicopters' X3 demonstrator [5] are the representative examples. JAXA also proposed compound helicopter design as shown in Figure 1 similar to Airbus Helicopters' X3 but utilizing two electric-driven anti-torque propellers at the wing-tips and an aft-mounted propeller for high speed propulsion. [6]

Figure 1: Conceptual drawing of a compound helicopter

When compound helicopters are flying at high speed, sonic barrier exists on the advancing side. It is required to reduce the rotor speed to keep the blade local speed less than that of the drag divergence speed. This increases the advance ratio further. For existing helicopters, the highest advance ratio generally does not exceed 0.4. While taking the X3 as an example of the compound helicopter, at the helicopter record breaking speed of 255 kt, assuming the rotor speed is reduced to 85% of the nominal RPM, the advance ratio is over 0.7. That means on the retreating side, reversed flow region may occupy over 70% of the blade. The rotor is unloaded by the added fixed wings and the flow conditions are significantly different from the conventional helicopters. The rotor design is expected to have a large room for further improvements to meet a new design objective of minimum rotor effective drag at high advance ratios.

CFD methods will play an important role for the optimization of the rotor blade for such a complex flight conditions, considering the lack of applicability of the traditional simple analytical methods. In JAXA, a comprehensive analysis tool chain for rotorcraft based on advanced CFD methodologies has been developed. [7] The CFD/CSD coupling solver, rFlow3D code, has been extensively verified with existing model rotor wind tunnel test data such as HART-II [8] and JMRTS experimental data. [9] The applicability of this code to the full scale rotor where the Reynolds number is much larger has not been validated so far. With a new requirement to simulate the aerodynamics around the proposed high speed compound helicopter, validation of the CFD methods at high advance ratio conditions become crucially important.

There are only limited test data available to the public. The UH-60A experiments carried out at NASA [10-12] provide a valuable source to validate the CFD methods. A series of validation computations based on the UH-60A data has been performed using rFlow3D. The hovering performance of the UH-60A rotor, the performance of the rotor in forward flight, and also the performance of the rotor at high advance ratio from a slowed-rotor test are compared between the

predictions and test data.

## 2. NUMERICAL METHODOLOGIES

In the rFlow3D code, a three dimensional moving overlapping grid method is adopted. [13] Euler, thin-layer Navier-Stokes, and full Navier-Stokes equations in an Arbitrary Lagrangian Eulerian (ALE) form can be solved using Finite Volume Method (FVM). The full N-S equation in ALE form is shown in Eq. 1, where **U** is the conservative flow variable vector and $\mathbf{F}^i$ and $\mathbf{F}^v$ are inviscid and viscous flux vector respectively. *V(t)* is the time-varying cell volume and *S(t)* is the time-varying cell boundary. **n** is the normal vector to the cell surface.

$$\frac{\partial}{\partial t}\int_{V(t)}\mathbf{U}dV+\oint_{S(t)}\left(\mathbf{F}^i-\mathbf{F}^v\right)\cdot\mathbf{n}dS=0 \tag{1}$$

where,

$$\mathbf{U}=\begin{bmatrix}\rho\\ \rho\mathbf{v}\\ \rho e\end{bmatrix},$$

$$\mathbf{F}^i\cdot\mathbf{n}=\begin{bmatrix}\left(\mathbf{v}-\dot{\mathbf{x}}\right)\cdot\mathbf{n}\rho\\ \left(\mathbf{v}-\dot{\mathbf{x}}\right)\cdot\mathbf{n}\rho\mathbf{v}+p\mathbf{n}\\ \left(\mathbf{v}-\dot{\mathbf{x}}\right)\cdot\mathbf{n}\rho e+p\mathbf{v}\cdot\mathbf{n}\end{bmatrix},$$

$$\mathbf{F}^v\cdot\mathbf{n}=\begin{bmatrix}0\\ \boldsymbol{\tau}\cdot\mathbf{n}\\ \left(\boldsymbol{\tau}\cdot\mathbf{v}-\mathbf{q}\right)\cdot\mathbf{n}\end{bmatrix}$$

The all-speed numerical scheme SLAU (Simple Low-dissipation AUSM) [14] with extension to three dimensional moving grids (referred as mSLAU) is adopted. [15] It is very suitable for the flow calculation around a rotary wing, where the local flow speed may vary from very low on the root area to transonic at the tip. Combining SLAU with a Fourth-order Compact MUSCL TVD (FCMT) interpolation scheme, [16] fourth-order spatial accuracy is obtained in shock free regions. Implicit LU-SGS and Dual-Time-Stepping method [17] are used for time integration on blade grids. Yet for the background grids, explicit four stages Runge-Kutta time integration method [18] is used.

Turbulence models such as Spalart-Allmaras model without the ft2 term (SA-noft2) [19] and Menter SST k-ω model (SST) [20] are incorporated in the rFlow3D code

The numerical methodologies adopted in the overlapping grid solver rFlow3D are summarized in Table 1. A sample of the overlapping grid system is shown in Figure 2. The grid around a UH-60A rotor blade is shown in Figure 3. The Renolds number based on the blade chord length ranges from $1.99\times10^6$ to $1.19\times10^7$. The minimum grid height on the blade surface is less than $y^+=1$ for following RANS calculations.

Table 1: Numerical Methodologies in rFlow3D

| rFlow3D CFD Methodologies | |
|---|---|
| Governing Eqs. | RANS |
| Advection terms | mSLAU (modified SLAU) |
| Reconstruction | FCMT (Fourth Order Compact MUSCL TVD) |
| Viscous terms | 2nd order central difference |
| Time integration | Background grid: Explicit four-stages Runge-Kutta<br>Blade grid: Dual-time stepping, LU-SGS |
| Turbulence model | Spalart-Allmaras model without ft2 term (SA-noft2) |

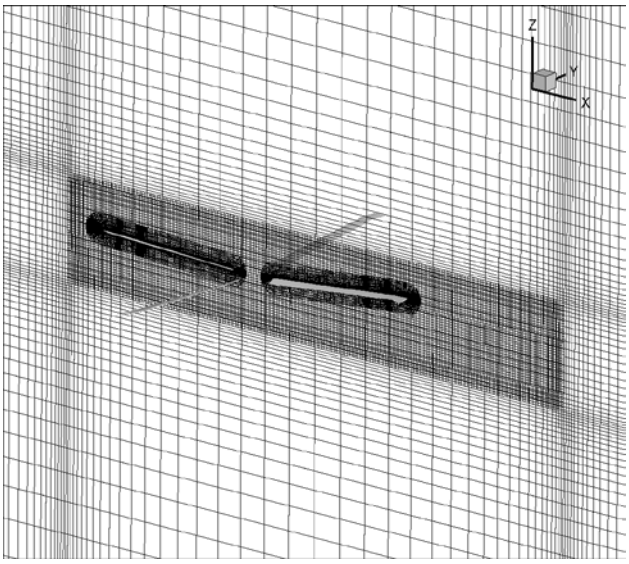


Figure 2: Moving overlapping grids

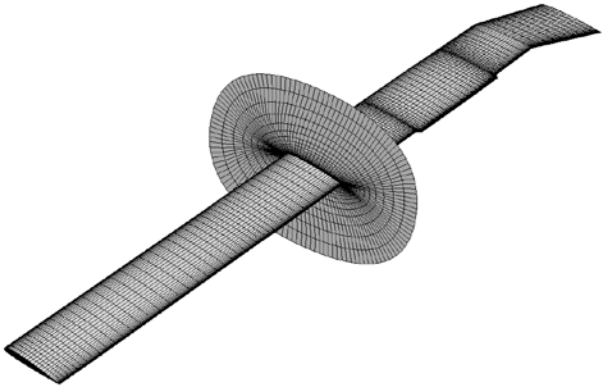

Figure 3: Grid around the UH-60A rotor blade

The trim adjustment algorithm in the rFlow3D has been updated with the control derivatives estimated based on a table of the aerodynamic coefficients, which was previously based on a constant lift gradient. This does improve the trim convergences especially at high advance ratios. A sample of the convergence histories of the trim controls to reach a target thrust and target roll and pitch moments in a forward flight condition is shown in Figure 4. For this rigid blade calculation, good convergence can be obtained after nearly 4 rotor revolutions.

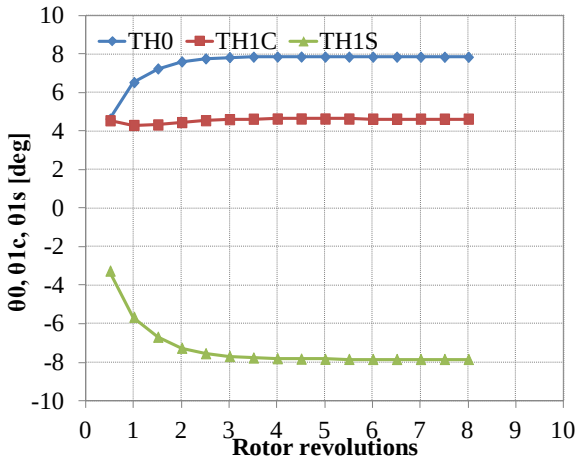


Figure 4: A sample of convergence histories of the trim cootnrols

## 3. RESULTS AND DISCUSSIONS

### 3.1. Hover Performance

A hover test for tip Mach number of 0.65 is compared as shown in Figure 5 for Figure of Merit (FM) and in Figure 6 for the torque vs thrust. Rigid rotor blade is assumed and the fuselage is not considered for all the computations in this paper.

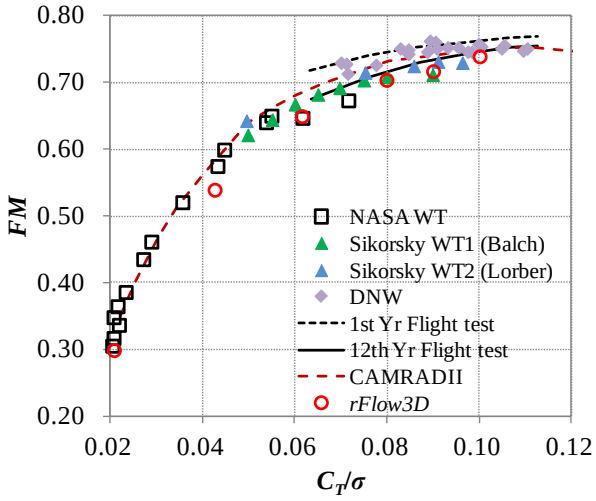


Figure 5: Figure of Merit vs Thrust comparison

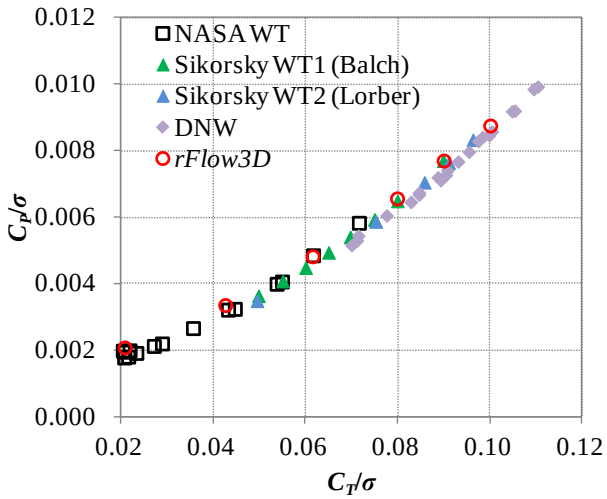


Figure 6: Torque vs Thrust curve comparison

The test and analysis data in these two plots except present results of rFlow3D are reproduced from reference [10]. It can be seen that very good agreements of the rFlow3D predictions with the NASA wind tunnel data are obtained.

### 3.2. Forward Flight

The test conditions for forward flight are based on reference [21-23] at shown in Table 2. The flapping angles at μ=0.15 and 0.37 are not explicitly given in the references, so the linearly interpolated values are used as written in red letters in Table 2. The target thrust with advance ratio is shown in Figure 7 and the hub moments are shown in Figure 8 where the computationally converged trim thrust and moments are also given.

Table 2: Forward flight conditions

| μ | $M_{tip}$ | $M_\infty$ | $\alpha_s$ (Corrected) | Target $C_T/\sigma$ | $\beta_0$ | $\beta_{1c}$ | $\beta_{1s}$ |
|---|---|---|---|---|---|---|---|
| 0.15 | 0.650 | 0.0975 | 0.90 | 0.09 | 3.9 | 1.8 | -0.1 |
| 0.20 | 0.650 | 0.1300 | -0.30 | 0.09 | 3.9 | 1.6 | 0.0 |
| 0.30 | 0.650 | 0.1950 | -3.49 | 0.09 | 3.9 | 1.1 | 0.3 |
| 0.37 | 0.650 | 0.2405 | -6.74 | 0.09 | 3.9 | 0.8 | 0.6 |
| 0.40 | 0.650 | 0.2600 | -7.60 | 0.09 | 3.9 | 0.6 | 0.6 |

(Note: Shaft and flappling angles are in degrees)

The collective and cyclic pitch angles for trim to the target thrust and moments are shown in Figure 9 and 10 respectively. There are offsets in the collective pitch angles about 2 degrees between the experiment and prediction. The main cause is considered as the lack of elastic torsional deformations. Also the bending of the trim tabs is not simulated in current computations. The trend of change with advance ratio agrees with the experiment well. Also, offsets of 1 to 2 degrees are

observed in the lateral cyclic pitch angles, while the longitudinal cyclic pitch angles match the experimental settings excellently.

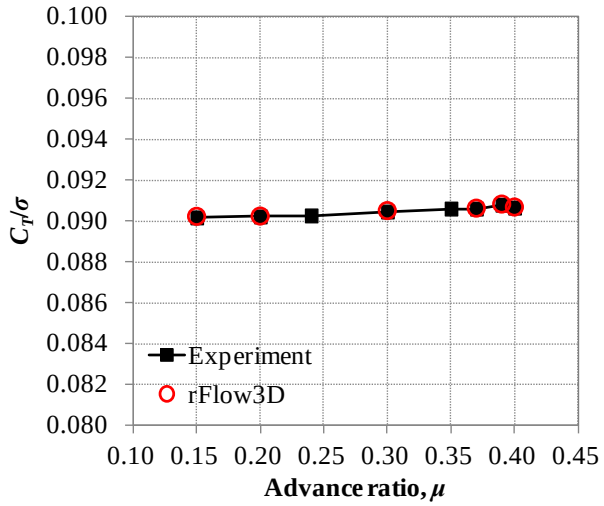


Figure 7: Target thrust in forward flight

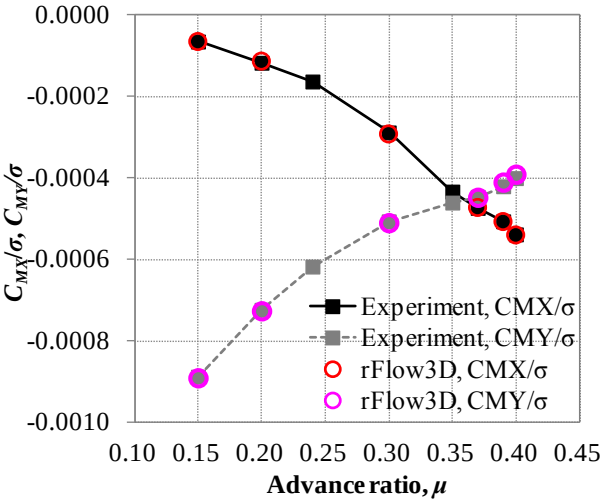


Figure 8: Target hub moments in forward flight

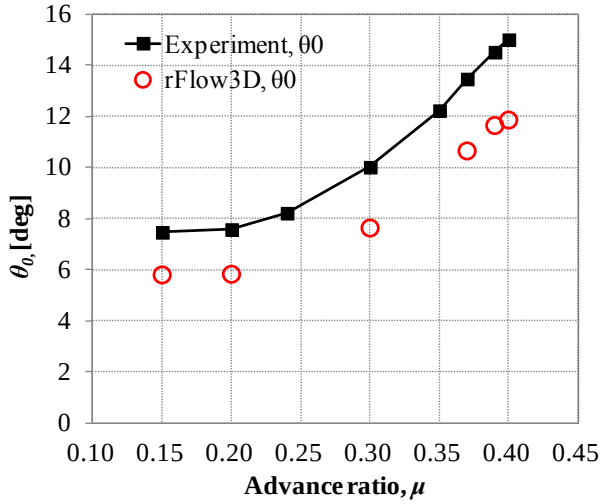


Figure 9: Collective pitch angle for trim

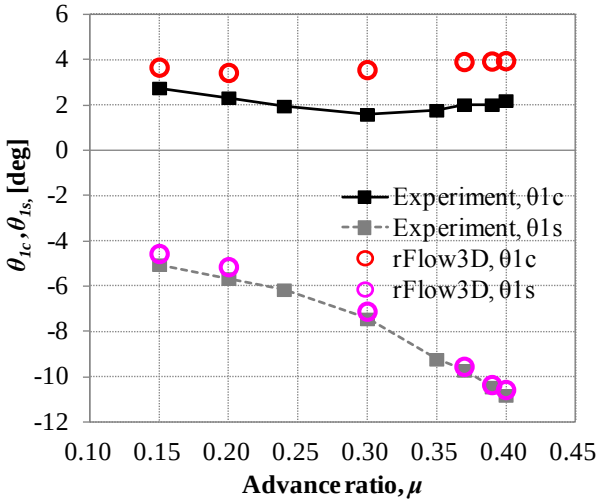


Figure 10: Cyclic pitch angles for trim

Comparison of the rotor propulsive X force is shown in Figure 11. Excellent agreements are found between the prediction and experiment. It is worthnoting that the drop in propulsive force from μ=0.39 to μ=0.4 is also accurately predicted.

The power coefficient with advance ratio is shown in Figure 12. Good agreement is found till moderate advance ratio about 0.3 but the prediction under-estimate the power about 10% when the advance ratio further increases up to 0.4.

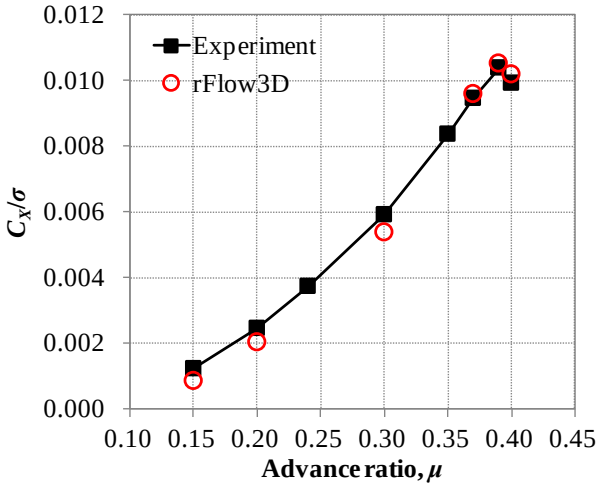


Figure 11: X force comparison

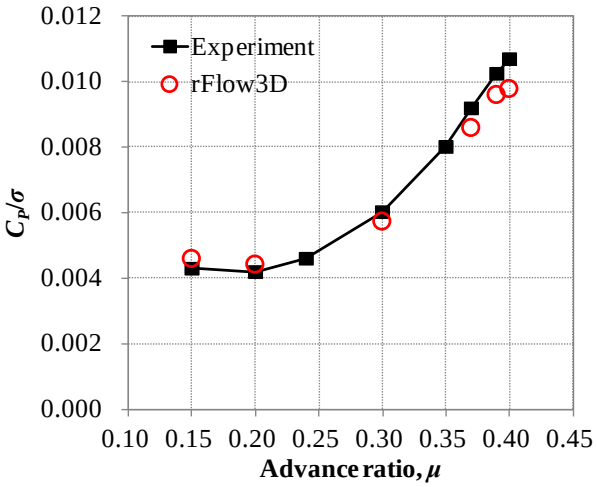


Figure 12: Power coefficient comparison

The sectional normal force coefficients at r/R=0.92 are compared in Figure 13. The trend with advance ratio is well captured with the dips (negative loading at high advance ratio) move to azimuth angle of 90 degrees.

On the other hand, the sectional pitching moment as shown in Figure 14 dips toward 180 degrees when advance ratio increases and this feature is also captured in the prediction.

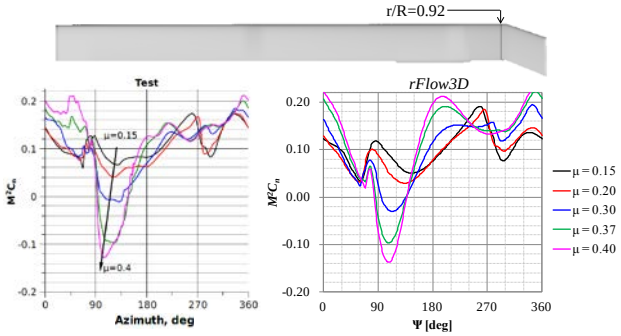


(a) test data of M2Cn (b) Predicted M2Cn

Figure 13: Comparison of normal force coefficient at r/R=0.92

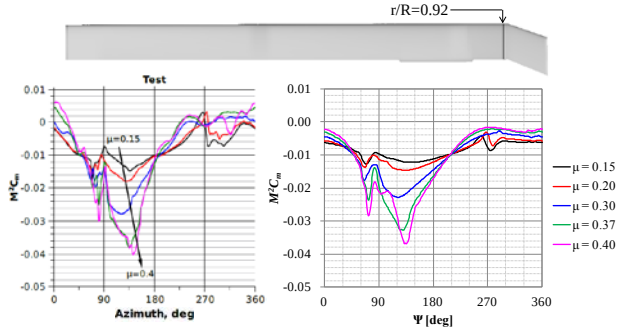


(a) test data of M2Cm (b) Predicted M2Cm

Figure 13: Comparison of sectional pitching moment coefficient at r/R=0.92

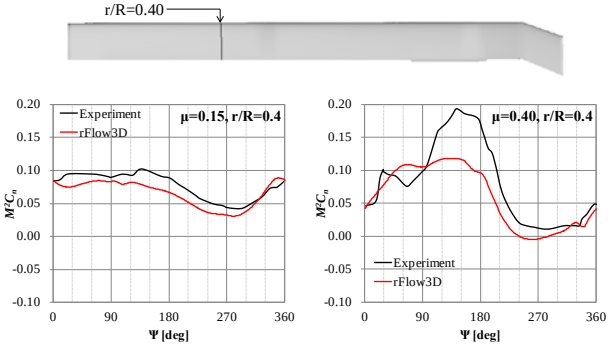


Figure 14: Normal lift variation at r/R=0.4 for advance ration of 0.15 (left) and 0.4 (right)

### 3.3. High Advance Ratio Flight

High advance ratio simulations are carried out for three experimental thrust cases as shown in Figure 15. [12, 24] For the trim conditions, the thrust is set to the experimental data with zero hub moments. The 1/rev flappling angles are set to zero with the coning angle calculated from Eq. 2. The shaft angle in the experiment was set to zero degrees, but small wind tunnel corrections calculated from Eq. 3 as described by Datta. [12]

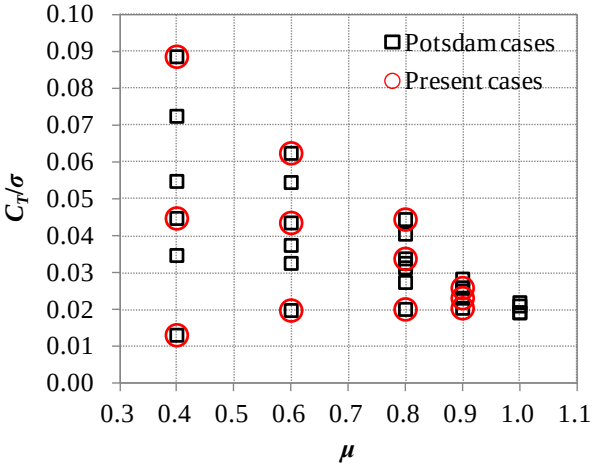


Figure 15: Simulated cases of slowed rotor

$$\beta_0 = \frac{2}{3}\gamma\left(\frac{C_T/\sigma}{A}\right) - \frac{3/2\, gR}{(\Omega R)^2}[radians] \quad (2)$$

$$\Delta\alpha = 8.6101\left(\frac{C_N}{\mu^2}\right)[\deg] \quad (3)$$

Representative flowfields of high m rotor are shown

in Figure 16. The reversed flow on the retreating side can be observed.

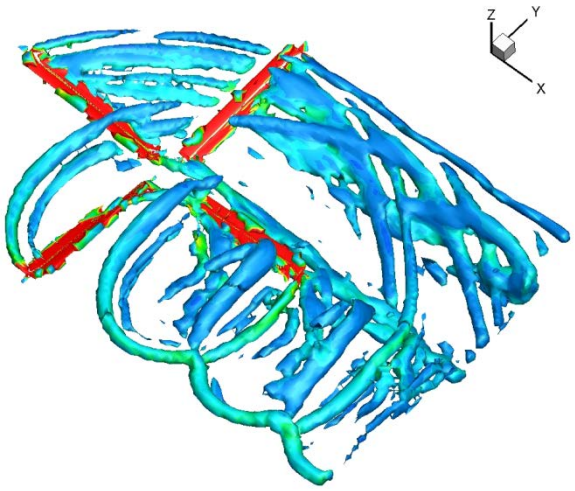

(a) $\mu$=0.4, $C_T/\sigma$=0.08

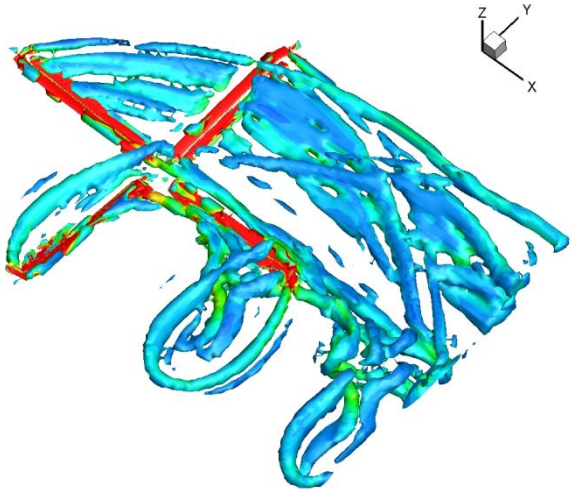

(b) $\mu$=0.6, $C_T/\sigma$=0.06

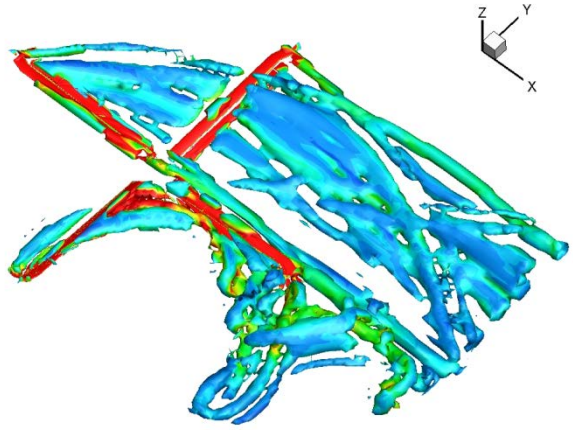

(c) $\mu$=0.8, $C_T/\sigma$=0.04

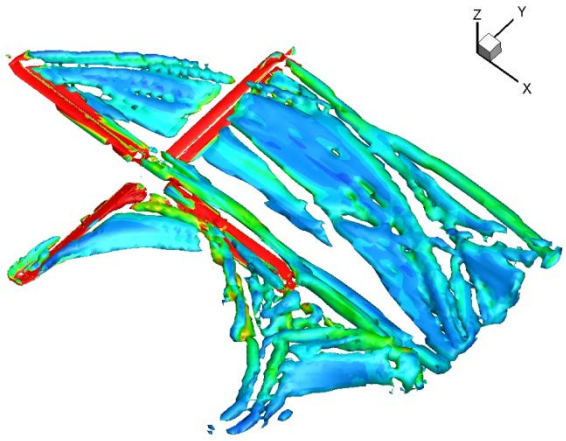

(d) $\mu$=0.9, $C_T/\sigma$=0.02

Figure 16: Rotor wake trajectories for different advance ratios

As shown in Figure 17, the CP increases with CT for m=0.4 and 0.6. But for high m of 0.8, 0.9, the CP decreases with CT. This trend is captured in the prediction. But the discrepancies of CP with experiemental data grow at high advance ratios. The cause of these significant discrepancies are considered mainly due to the uncerntainty of the rotor trim. With the power component from the propulsive X force removed as shown in Eq. 4, the so-called effective rotor drag coefficient $C_{DE}$ can be obtained. As shown in Figure 18, excellent agreements between the measurement and prediction are found. Because the estimation of the effective rotor drag is crucial for the compound helicoter where the propulsive force will mainly provided by additional propellers, it is concluded the numerical methods in rFlow3D are satisfactory to evaluate the rotor performance also in high advance ratio flight.

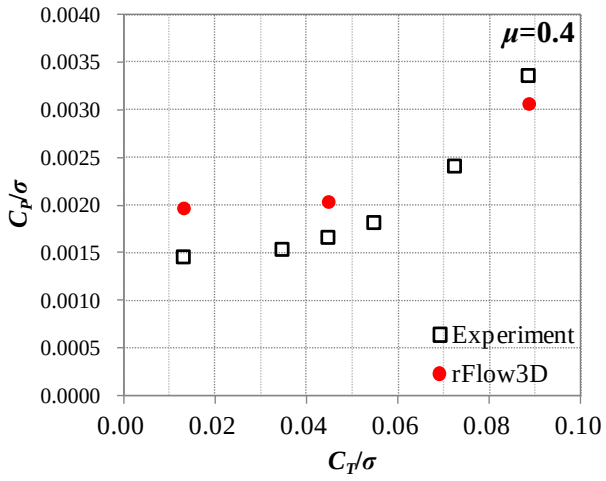


Figure 17 (a) CT-CP for μ=0.4

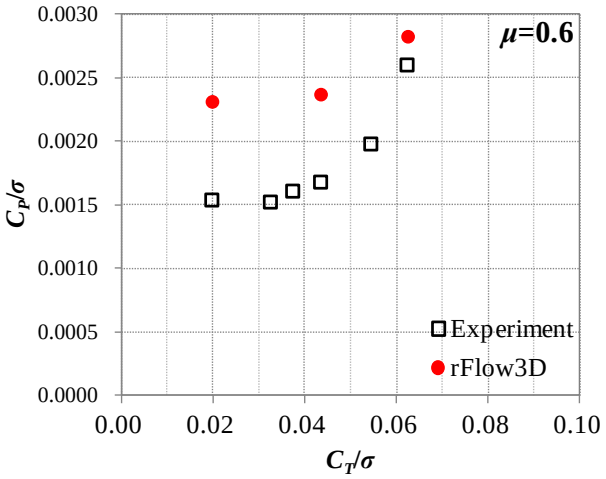


(b) CT-CP for μ=0.6

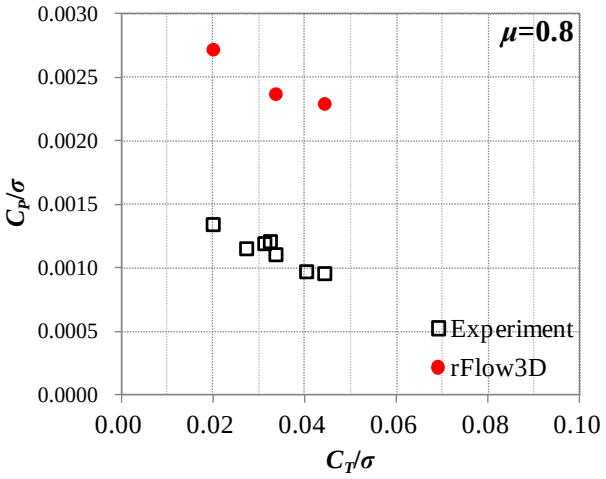


(c) CT-CP for μ=0.8

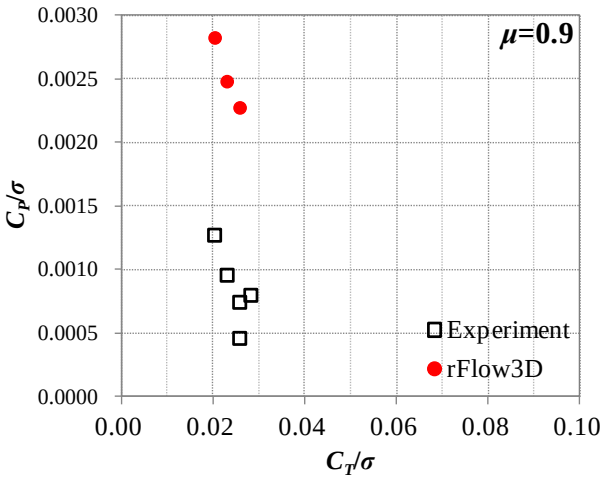


(d) CT-CP for μ=0.9

Figure 17: CT-CP curves for high μ rotor

(4) $$C_{DE} = \left(C_{Pi} + C_{P0}\right)/\mu = C_P/\mu - C_X$$

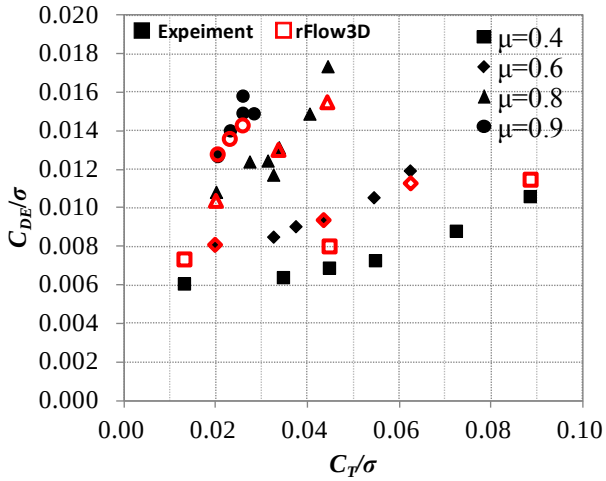


Figure 18: Comparisons of effective rotor drag

## 4. CONCLUSIONS AND FUTURE WORKS

Validation of the rFlow3D code developed at JAXA has been carried out with the published available UH-60A test data in hover and forward flight. Also, the slowed rotor conditions are simulated to investigate the applicability of this code at high advance ratios. Although the elastic deformation of the blade is not considered at this point, good agreement of the aerodynamic performance is obtained compared with the experimental data.

The rFlow3D code has been expanded to treat multiple rotors and propellers as shown in Figure 19. Using multiple refined inner background grids, flowfield around each rotor or propeller can be solved with desired resolutions. A sample of the flowfileds around a model compound helicopter is shown in Figure 20.

As future works, further validation of the CFD/CSD coupling analysis with experimental elastic blade data will be carried out. Also, trim of a complete rotorcraft will be incorporated. Studies and understanding of the interactions between rotors, wings, and propellers will be highly beneficial for the development of future rotorcraft.

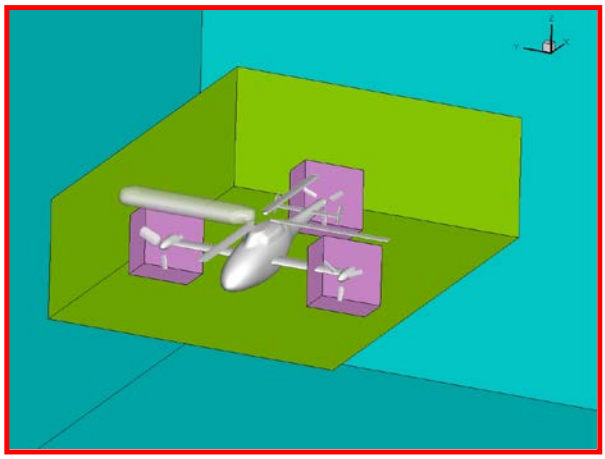

Figure 19: Overset grids for a complete compound helicopter with multiple rotors and propellers

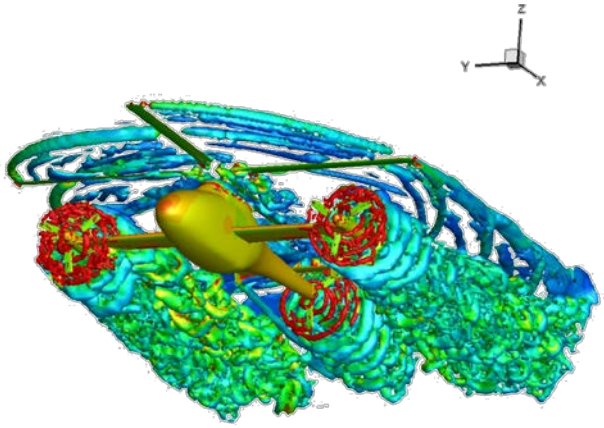

Figure20: Flowfield around a sample compound helicopter

## COPYRIGHT STATEMENT



## REFERENCES

[1] Orchard, M.N. and Newman, S.J., The compound helicopter versus tilt rotor: Europe's shortcut to the future. 26th ERF, Hague, NL, Sept. 14 - 16, 2000.

[2] Bagai, A., Aerodynamic Design of the X2 Technology DemonstratorTM Main Rotor Blade, 64th AHS Annual Forum, Montreal, Canada, April 29-May 1, 2008.

[3] Blackwell, R. and Millott, T., Dynamics Design Characteristics of the Sikorsky X2 Technology Demonstrator Aircraft. In American Helicopter Society 64th Annual Forum, Montreal, Canada, 2008.

[4] Walsh, D., Weiner, S., Bagai, A., Lawerence, T. and Blackwell. R., Development Testing of the Sikorsky X2 Technology Demonstrator, 65th AHS Annual Forum, Grapevine, TX, 2009.

[5] Nelms, D., Aviation Week Flies Eurocopters X3, Aviation Week & Space Technology, Vol. 174, No. 24, Jul. 9, 2012.

[6] Tanabe, Y. Aoyama, T., Kobiki, N., Sugiura, M., Miyashita R., Sunada S. Kawachi K. and Nagao, M., A Conceptual Study of High Speed Rotorcraft, 40th ERF, Southampton, UK, Sept. 2-5, 2014.

[7] Tanabe, Y., Saito S., and Sugawara, H., Construction and Validation of an Analysis Tool Chain for Rotorcraft Active Noise Reduction, 38th ERF, Amsterdam, NL, Sept. 4-7, 2012.

[8] Yu, Y.H., Tung, C., van der Wall, B., Pausder, H.-J., Burley, C., Brooks, T., Beaumier, P., Delrieux, Y., Mercker, E., & Pengel, K., The HART-II Test: Rotor Wakes and Aeroacoustics with Higher-Harmonic Pitch Control (HHC) Inputs - The Joint German/French/Dutch/US Project -, AHS 58th Annual Forum, Montreal, Canada, June 11-13, 2002

[9] Sugawara, H., Tanabe, Y. and Saito, S., Influence of Fuselage on Blade-Vortex Interaction Based on JMRTS Database, 1st Asian/Australian Rotorcraft Forum, Busan, Korea, Feb. 12-15, 2012.

[10] Shinoda, P. M., Rotor Performance of a UH-60 Rotor System in the NASA Ames 80- by 120-Foot Wind Tunnel, 58th AHS Annual Forum, Montreal, Canada. June 11-13, 2002.

[11] Norman, T., Peterson, R., Shinoda, P., and Datta, A., Full-Scale Wind Tunnel Test of the UH-60A Airloads Rotor, American Helicopter Society 67th Annual Forum Proceedings, 2011.

[12] Datta,A., Experimental Investigation and Fundamental Understanding of a Slowed UH-60A Rotor at High Advance Ratios, the American Helicopter Society 66th Annual Forum, Virginia Beach, VA, May 3-5, 2011.

[13] Tanabe, Y., Saito, S., Takayama, O., Sasaki, D.

and Nakahashi, K., A New Hybrid Method of Overlapping Structured Grids Combined with Unstructured Fuselage Grids for Rotorcraft Analysis, 36th European Rotorcraft Forum, Paris, France, September 9-11, 2010.

[14] Shima, E., and Kitamura, K., “On New Simple Low-Dissipation Scheme of AUSM-Family for All Speeds,” 47th AIAA Aerospace Sciences Meeting, Orlando, FA, January 5-8 2009, AIAA Paper 2009-136.

[15] Tanabe, Y. and Saito, S., “Significance of All-Speed Scheme in Application to Rotorcraft CFD Simulations,” The 3rd International Basic Research Conference on Rotorcraft Technology, Nanjing, China. October, 2009.

[16] Yamamoto, S. & Daiguji, H., “Higher- Order-Accurate Upwind Schemes for Solving the Compressible Euler and Navier-Stokes Equations,” Computers & Fluids, Vol.22, No.2/3, pp.259-270, 1993.

[17] Zhang, L.P. and Wang, Z.J., “A Block LU-SGS Implicit Dual Time-Stepping Algorithm for Hybrid Dynamic Meshes,” Computers & Fluids, Vol.33, pp.891–916, 2004.

[18] Arnone, A., Liou, M.S. and Povinelli, L. A., "Multigrid Time-Accurate Integration of Navier-Stokes Equations," NASA TM-106373, November 1993.

[19] Spalart, P. R., and Allmaras, S. R., “A One-Equation Turbulence Model for Aerodynamic Flows,” AIAA-92-0439, January 6-9, 1992.

[20] Menter, F. R., "Two-Equation Eddy-Viscosity Turbulence Models for Engineering Applications," AIAA Journal, Vol. 32, No. 8, August 1994, pp. 1598-1605.

[21] Romander, E., Correlating CFD Simulation with Wind Tunnel Test for the Full-Scale UH-60A Airloads Rotor, the American Helicopter Society 67th Annual Forum, Virginia Beach, VA; May 3–5, 2011.

[22] Yeo, H. and Romander, E., “Loads Correlation of a Full-Scale UH-60A Airloads Rotor in a Wind Tunnel,” American Helicopter Society 68th Annual Forum Proceedings, 2012.

[23] Lee-Rausch, E. M., and Biedron, R. T., FUN3D Airload Predictions for the Full-Scale UH-60A Airloads Rotor in a Wind Tunnel, AHS 69th Annual Forum, Phoenix, Arizona, May 21–23, 2013.

[24] Potsdam, M., Datta, A. and Jayaraman, B., Computational Investigation and Fundamental Understanding of a Slowed UH-60A Rotor at High Advance Ratios, American Helicopter Society 68th Annual Forum, Fort Worth, TX, May 1-3, 2012.